Table of Contents

SUPPLEMENTAL MATERIALS AND METHODS

Co-immunolocalization and Confocal Microscopy

For co-immunolocalization studies, YFP was detected using a rabbit anti-GFP antibody (Invitrogen) or a chicken anti-GFP antibody (Abcam) at 1:500. The mouse anti-calbindin antibody (Sigma) was used at 1:100, the mouse anti-bassoon antibody (Stressgen) was used at 1:500, the mouse anti-PSD95 antibody (ABR) was used at 1:100, the mouse anti-neurofilament H&M antibody (Millipore clone NP1) was used at 1:500, the mouse anti neurofilament (Millipore clone DA2) antibody was used at 1:1000, the rabbit anti neurofilament heavy chain (Millipore Cat # AB5539SP) antibody was used at 1:1000 and the mouse anti-PKCα antibody (Upstate) was used at 1:5000. To visualize the anti-GFP antibodies, we used goat anti-rabbit-Alexa488 or goat anti-chicken-Alexa488 antibodies (invitrogen) at 1:500. To visualize the other antigens, we used donkey anti-mouse-biotin antibody (Vector labs) at 1:500 followed by ABC (Vector labs) and Tyramide Cy3 detection. Nuclei were stained with Dapi.

Electron Microscopy and Lead Citrate Staining

All procedures for TEM and lead citrate staining have been described previously (1). A detailed procedure is presented in supplemental information. Animals were anesthetized with avertin until a loss of deep tendon reflexes. Transcardial perfusion was performed with carboxygenated Ames Medium supplemented with 40 mM glucose to clear the vasculature, followed by perfusion with Sorenson's phosphate buffer pH 7.2 with 2% EM grade paraformaldehyde and 1% EM grade glutaraldehyde. Eyes were then harvested, a slit was made in the cornea to aid in diffusion, and the tissue was placed in 3%

glutaraldehyde in Sorenson's phosphate buffer overnight. Tissue was washed with 0.2M cacodylate buffer in 5% sucrose, post-fixed in 1% OsO_4, embedded, sectioned, and viewed by transmission electron microscopy.

For EM imaging of alkaline phosphatase, we developed a modification of the protocol described by Contini and Raviola (2). Animals were perfusion-fixed as described above and the eyes were harvested. Retinae were then removed, embedded in 4% LMP agarose/1X PBS and 100 μm vibratome sections prepared. The sections were then placed in 3% glutaraldehyde for 30 min, rinsed in PBS buffer, heated in PBS at 65° C for 30 min, and thoroughly rinsed with 5% sucrose in 0.2 M cacodylate buffer to eliminate phosphate ions. Sections were then incubated overnight with mild shaking in a beta-glycerophosphate, alkaline lead citrate solution(3). Samples were thoroughly rinsed in cacodylate buffer, and post-fixed in 3% glutaraldehyde. Selected samples were stained with osmium-ferrocyanide and uranly acetate; others were left unstained to better appreciate the alkaline phosphatase staining. Images were acquired on an FEI 200kv field beam electron microscope. For 3D reconstruction, sections were imaged and aligned and then imported into Imaris for visualization.

Automated Analysis of Horizontal Neuron Morphology

In our approach, we characterize the retinal neurons four main steps: (1) soma detection, (2) dendrite segmentation, (3) skeletonization and network analysis, and (4) feature extraction. We first localize each individual soma in the large-scale 3D confocal imagery by using the morphological operators and active contours. By using each soma position as a seed point, we automatically determine an appropriate threshold to segment dendrites

in each neuron. Then, the skeletonization and network analysis step generates the morphological structures of segmented dendrites, and shape-based features are extracted from network representation of each neuron to characterize each neuron. More details about these steps are given in the following sections.

1.1 Soma detection

We first filter the image by an erosion operator with a spherical structuring element whose radius is equal to size of the minimum volume enclosing the typical soma. Then, adaptive thresholding converts the grayscale erosion resultant image to a binary image to separate the foreground and background regions. The adaptive threshold is set to keep image regions whose mean intensity value is greater than the 50% of the mean of the resultant image. After thresholding, connected component analysis labels all separate image regions as different somas using 26-connectivity, and the centroid of each soma is computed. By using each soma centroid as a seed point, an active contour algorithm automatically determines the boundary of each soma based on the Chan-Vese energy [9].

1.2 Dendrite segmentation

We utilize the dendrite segmentation method proposed in [7] which searches to detect the volumetric explosion of the object of interest as a high initial threshold value is gradually decreased. In this approach, the threshold value is initialized as the maximum intensity value within the soma of interest and gradually steps down until reaching a value where the connected voxels to the soma of interest will suddenly “explode” in size as large amounts of background voxels become connected to the soma of interest. The optimal threshold is found by backing off slightly from the value at which the volumetric explosion occurred. More details are presented in [7]. This procedure is repeated for

every soma in the dataset, and segmentation results of each neuron are converted to a binary image.

1.3 Skeletonization and network analysis

We utilize a modified version of the iterative 3-D skeletonization algorithm proposed in [10]. The original thinning algorithm peels iteratively the outermost layer of the binary image of the dendritic tree until only the central voxels of dendrites remain. In this approach, the voxels which have the least number of neighbors are defined as outmost layer and deleted first. Kerekes et al. [7] extended this approach by taking the intensity values of the corresponding voxels into account for the skeletonization of the grayscale dendrite segmentation image. Since dimmest voxels in the outmost layer are deleted first, this approach keeps the brightest voxels of dendrites in the final skeleton.

After skeletonization of each dendritic segment, we establish the network representation of the dendritic tree with a combination of nodes and edges to extract the morphological structure of dendrites. Skeleton voxels with one neighbor (end point) and voxels with at least three neighbors (branch points) are identified as *nodes* to represent the branching points of the dendrites from either the soma or another dendritic segment. Each skeleton voxel which has exactly two neighbors is identified as a segment point, and connected segment points between two neighboring nodes are grouped to form an *edge* which represents the corresponding dendritic segment in the skeleton. Thus, the skeleton is converted to a system of edges and nodes.

1.4 Feature Extraction

Each retinal neuron has three types of dendrites: apical (extending upward), basal (extending downward), and horizontal, and each dendrite exhibits distinct morphological features (e.g., emanating point, angle, height). At postnatal day 6 (P6), the dendrites in a normal horizontal mouse neuron typically become horizontal and emanate from the top of soma (Fig. 1(a)). However, in the case of Rb-deficient mice, abnormal cell development can take place in the retina resulting in the formation of abnormal dendrite morphology (i.e., lingering apical or basal dendrites) and become evident at P6. The apical and basal dendrites emanate from top and bottom poles of the soma and extend to upper and lower retinal layers as shown in Fig.1 (b-c), respectively.

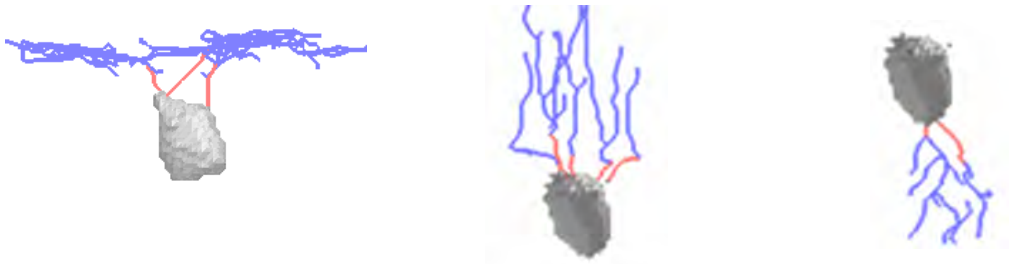

(a) (b) (c)

Skeleton examples for different types of dendrites and soma volume of retinal horizontal neuron, (a) horizontal dendrites, (b) apical dendrites, and (c) basal dendrites.

In order to characterize the morphology of dendrites and classify them as apical, basal and horizontal, we extract the following features from morphological structure of dendrites: (1) emanating point, (2) angles of dendritic segments with respect to emanating

point, (3) angles of dendritic segments with respect to previous dendritic segment, (4) length of dendrite, (5) height of dendritic segments in z-axis, (6) angle of best fitting plane, (7) distance to best fitting plane. Based on these extracted features, we introduce a probabilistic model that computes the probability of a dendrite to be apical, basal or horizontal. Finally, we classify each dendrite into different classes by comparing the probability of being apical, basal and horizontal.

Supplemental Fig. 1. Ectopic horizontal cell processes contain neurofilament. (A,B) Co-immunolocalization of YFP (green) and neurofilament (red) in P14 *Chx10-Cre;*$Rb^{Lox/+}$*;Rosa-YFP* or P14 *Chx10-Cre;*Rb^{LoxLox}*;Rosa-YFP* mouse retinae. Ectopic neurofilament horizontal cell axons (arrow in B) are often associated with regions where *Rb* has been inactivated (green immunofluorescence). **(C)** Co-immunolocalization of YFP (green) and calbindin (red) and neurofilament (pink) in P14 *Chx10-Cre;*$Rb^{Lox/Lox}$*;Rosa-YFP* mouse retinae. Arrow indicates an ectopic horizontal cell process that is associated with an *Rb*-deficient region (green) and is also expressing neurofilament. Nuclei are shown in blue. Abbreviations: ONL, outer nuclear layer; INL, inner nuclear layer; OPL, outer plexiform layer; IPL, inner plexiform layer; GCL, ganglion cell layer; Scale bars in A,B: 25μm and in C: 10μm.

Martins et al. Sup. Fig. 1

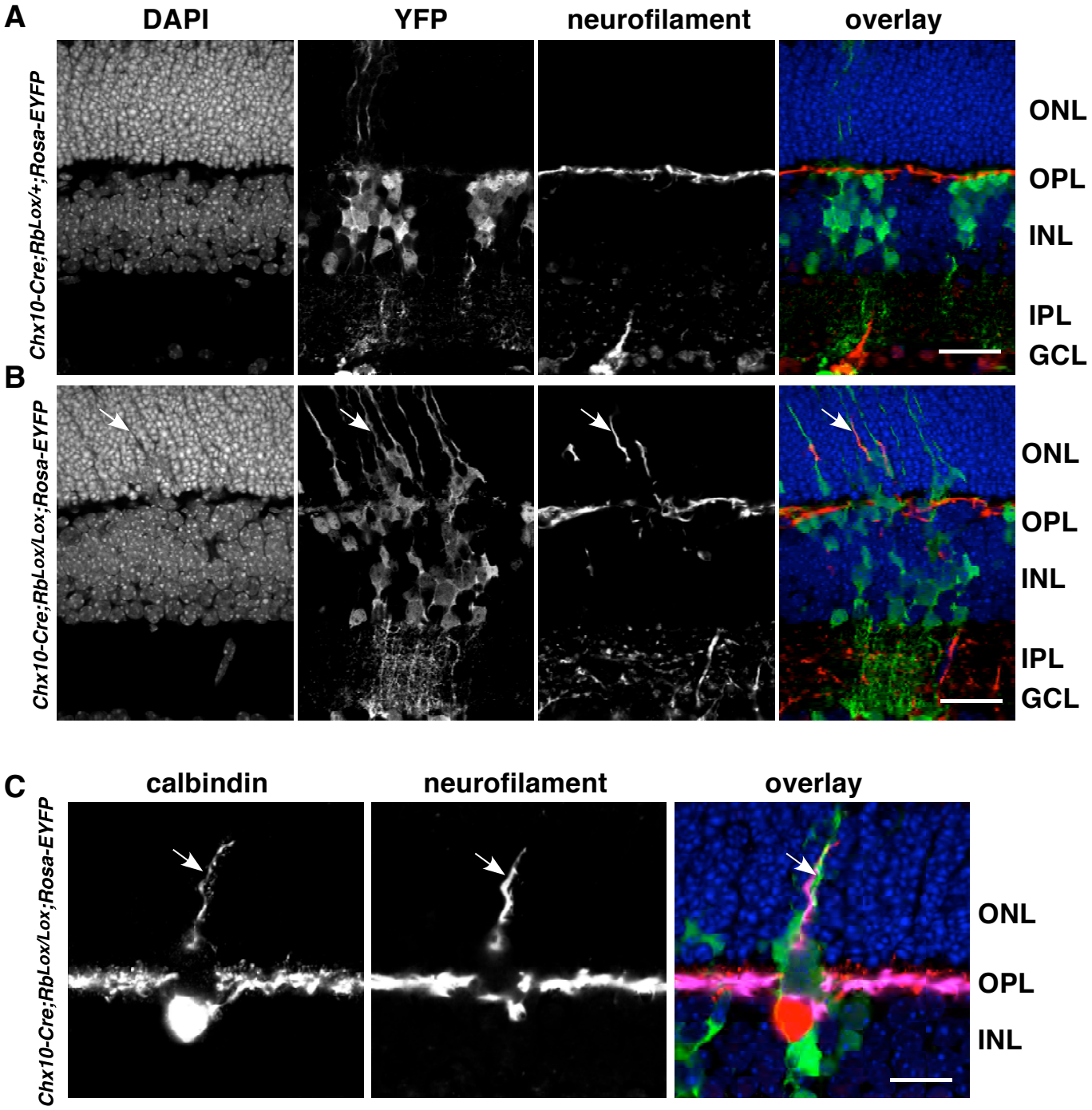

Supplemental Fig. 2. Cone bipolar cells are normal in *Rb*-deficient retinae. (A) Co-immunolocalization of YFP (green) and CaBP5 (red) in P14 *Chx10-Cre;*Rb^{LoxLox}*;Rosa-YFP* mouse retinae. Cone bipolar cells were clearly identified (arrow) but there was no evidence of ectopic dendrites in *Rb*-deficient regions of the retina labeled with YFP. **(B)** Co-immunolocalization of cone and rod bipolar cells from the mGluR6-GFP transgene (green) and rod bipolar cells labeled with PKC–α (red) in adult retinae. The arrow indicates a rod bipolar cell that is double positive for PKC–α and GFP while the open arrowhead indicates a cone bipolar cell that is negative for PKC–α and positive for GFP. Nuclei are shown in blue. **(C)** Two representative examples of GFP expression in live retinae at P19 from control *Chx10-Cre;*$Rb^{Lox/+}$*;mGluR6-GFP* and knockout *Chx10-Cre;*$Rb^{Lox/Lox}$*;mGluR6-GFP* P19 retinae. There is no evidence of ectopic bipolar processes from any of the stages analyzed or any of the fields characterized. Abbreviations: ONL, outer nuclear layer; INL, inner nuclear layer; OPL, outer plexiform layer; IPL, inner plexiform layer; GCL, ganglion cell layer; Scale bars in A,B: 25μm and in C: 10μm.

Martins et al. Fig. 2

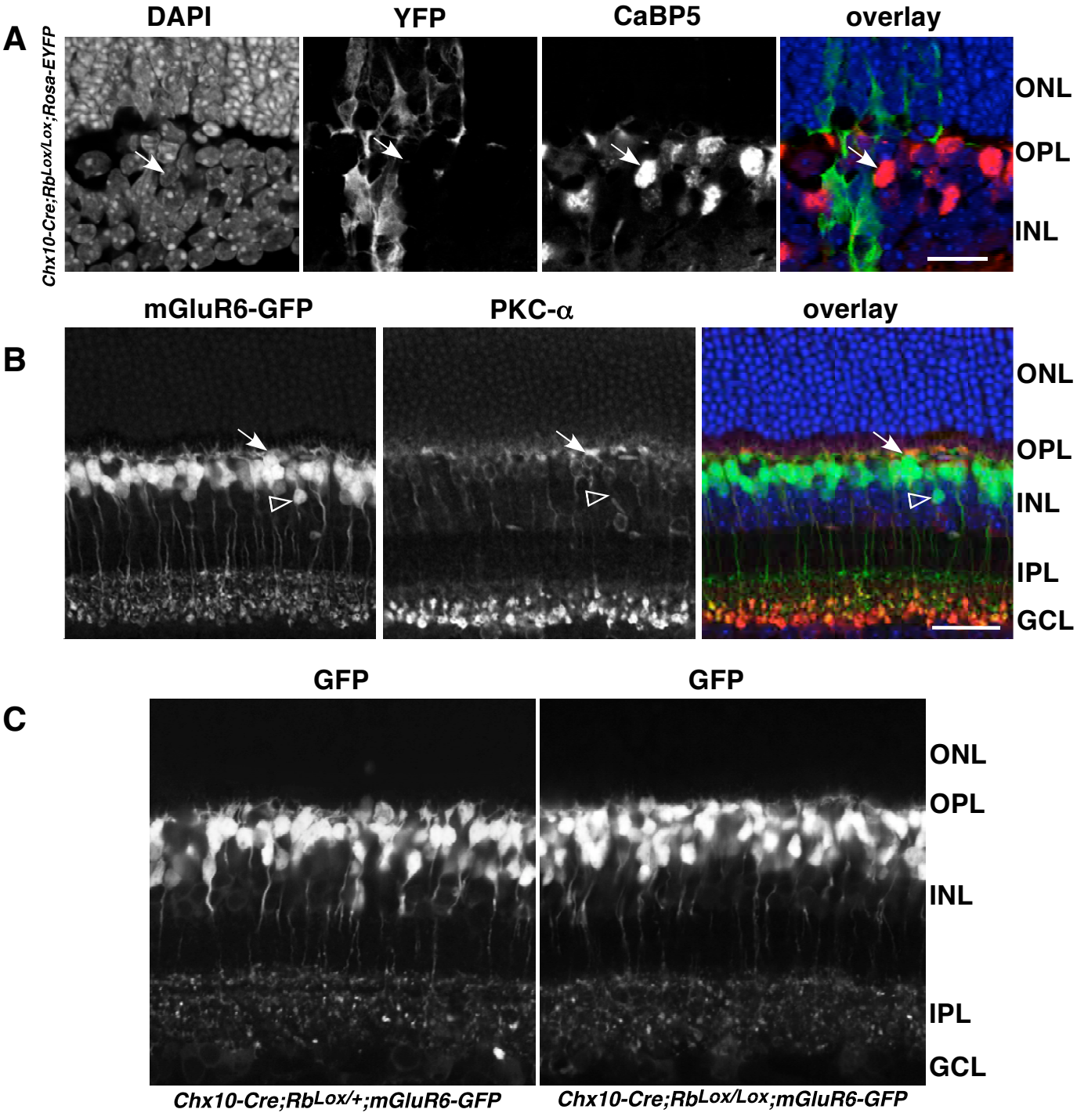

Supplemental Fig. 3. Horizontal neurons for ectopic synapses in the *Chx10-Cre;Rb$^{Lox/Lox}$* retinae. (A,B) Co-immunolocalization of YFP (green) and bassoon (red) in P21 *Chx10-Cre;Rb$^{Lox/Lox}$;Rosa-YFP* mouse retinae. Ectopic bassoon punctae (arrow in B) are often associated with regions where *Rb* has been inactivated (green immunofluorescence). **(C)** The association of ectopic bassoon punctae was scored with respect to YFP expressing columns of cells at P11-P14 and P18-P21. 100 individual columns were scored from 6 independent retinae at both stages of development. **(D)** In those columns that contained ectopic bassoon punctae, the number of punctae were scored at P11-P14 and P18-P21. Mean and standard deviation of scoring from the 6 independent retinae at each stage are presented in the histograms in (C,D). **(E,F)** Co-immunolocalization of YFP (green) and PSD95 (red) in P21 *Chx10-Cre;Rb$^{Lox/Lox}$;Rosa-YFP* mouse retinae. Ectopic PSD95 foci (arrow in F) are often associated with regions where *Rb* has been inactivated (green immunofluorescence). **(G)** The association of ectopic PSD95 foci was scored with respect to YFP expressing columns of cells at P11-P14 and P18-P21. 100 individual columns were scored from 6 independent retinae at both stages of development. **(H)** In those columns that contained ectopic PSD95 foci, the number of foci was scored at P11-P14 and P18-P21. Mean and standard deviation of scoring from the 6 independent retinae at each stage are presented in the histograms in (G,H). **(I-K)** 4-color confocal image of co-immunolocalization of YFP (green), calbindin (pink) and bassoon (red). Nuclei are shown in blue. YFP expression is shown in (J) and the co-localization of calbindin (gray) and bassoon (yellow) is shown in (K). Abbreviations: ONL, outer nuclear layer; INL, inner nuclear layer; OPL, outer plexiform

layer; IPL, inner plexiform layer; GCL, ganglion cell layer; HC, horizontal cell; Bip, bipolar neuron. Scale bars: 10μm.

Martins et al. Sup. Fig. 3

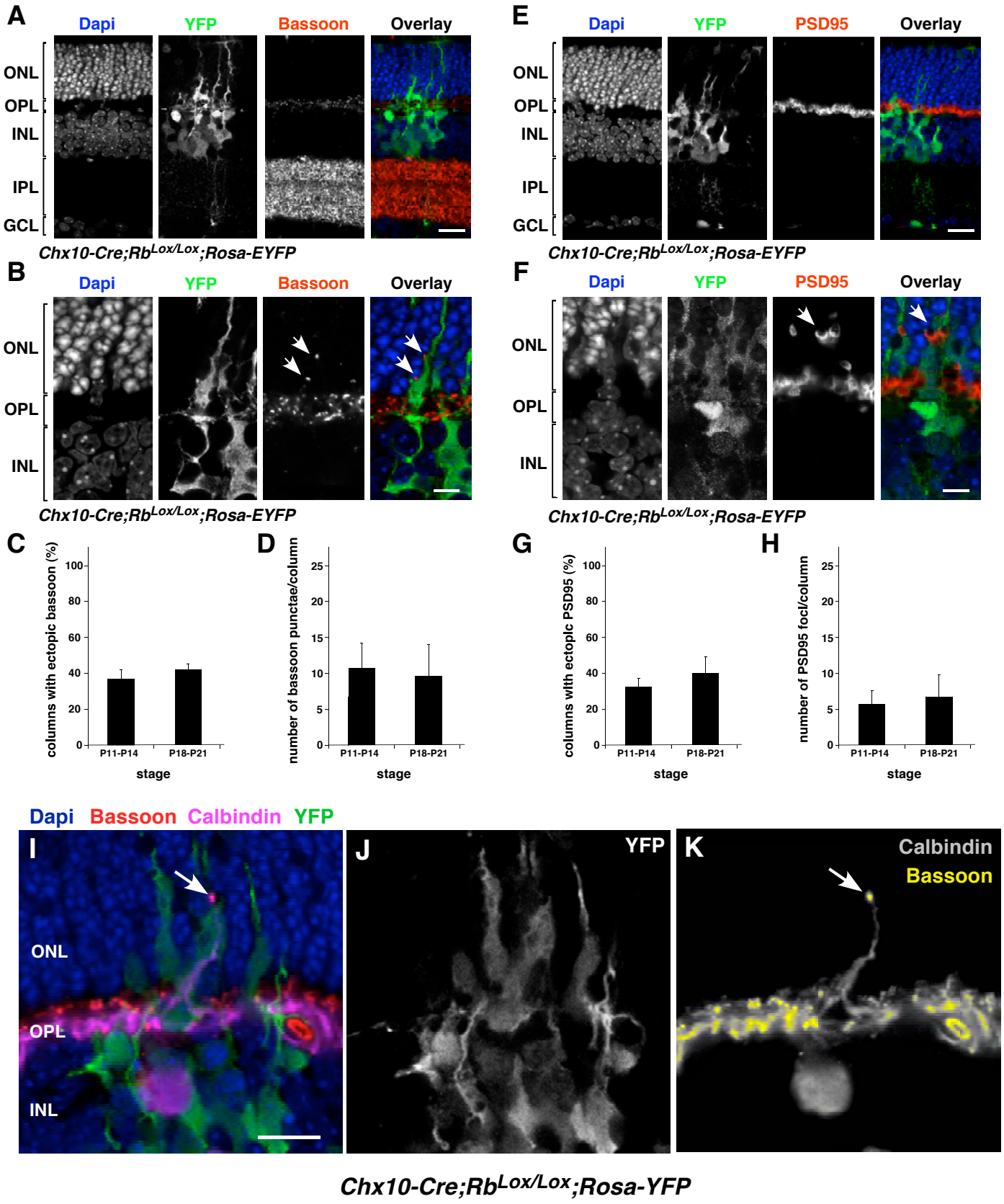

Supplemental Fig. 4. Genetic mosaic analysis of individual synapses in *Chx10-Cre;Rb$^{Lox/Lox}$;Z/AP* retinae. (A,B) Lead citrate staining of OPL synaptic triads from the *Chx10-Cre;Rb$^{Lox/+}$* retinae. In this retina, only the bipolar cells express ALPP from the *Chx10-Cre* transgene. Bipolar cell bodies, processes and dendrites in rod and cone triads were labeled. Arrows indicate bipolar dendrites lacking synaptic vesicles in rod terminals. **(C)** High resolution montage of a P21 *Chx10-Cre;Rb$^{Lox/Lox}$;Z/AP* retinae showing columns of cells that are labeled with ALPP and visualized by lead citrate staining. **(D)** Lead citrate staining of an ectopic synapse in the *Chx10-Cre;Rb$^{Lox/Lox}$;Z/AP* P21 retina showing a synaptic terminal surrounded by rod photoreceptor somata in the ONL. Dark labeling of the horizontal cell processes within the ectopic processes indicate that these processes were derived from an *Rb*-deficient horizontal cell. **(E,F)** Another example of lead citrate staining of an ectopic synapse in the *Chx10-Cre;Rb$^{Lox/Lox}$;Z/AP* P21 retina showing a synaptic terminal surrounded by rod photoreceptor somata in the ONL. The synaptic ribbon (sr) can be visualized as well as ALPP+ labeling in the cell processes (arrow) containing synaptic vesicles (open arrowheads). Abbreviations: OLM, outer limiting membrane; ONL, outer nuclear layer; INL, inner nuclear layer; OPL, outer plexiform layer; IPL, inner plexiform layer; GCL, ganglion cell layer; sr, synaptic ribbon; r, rod terminal; c, cone terminal.

Martins et al. Sup. Fig. 4

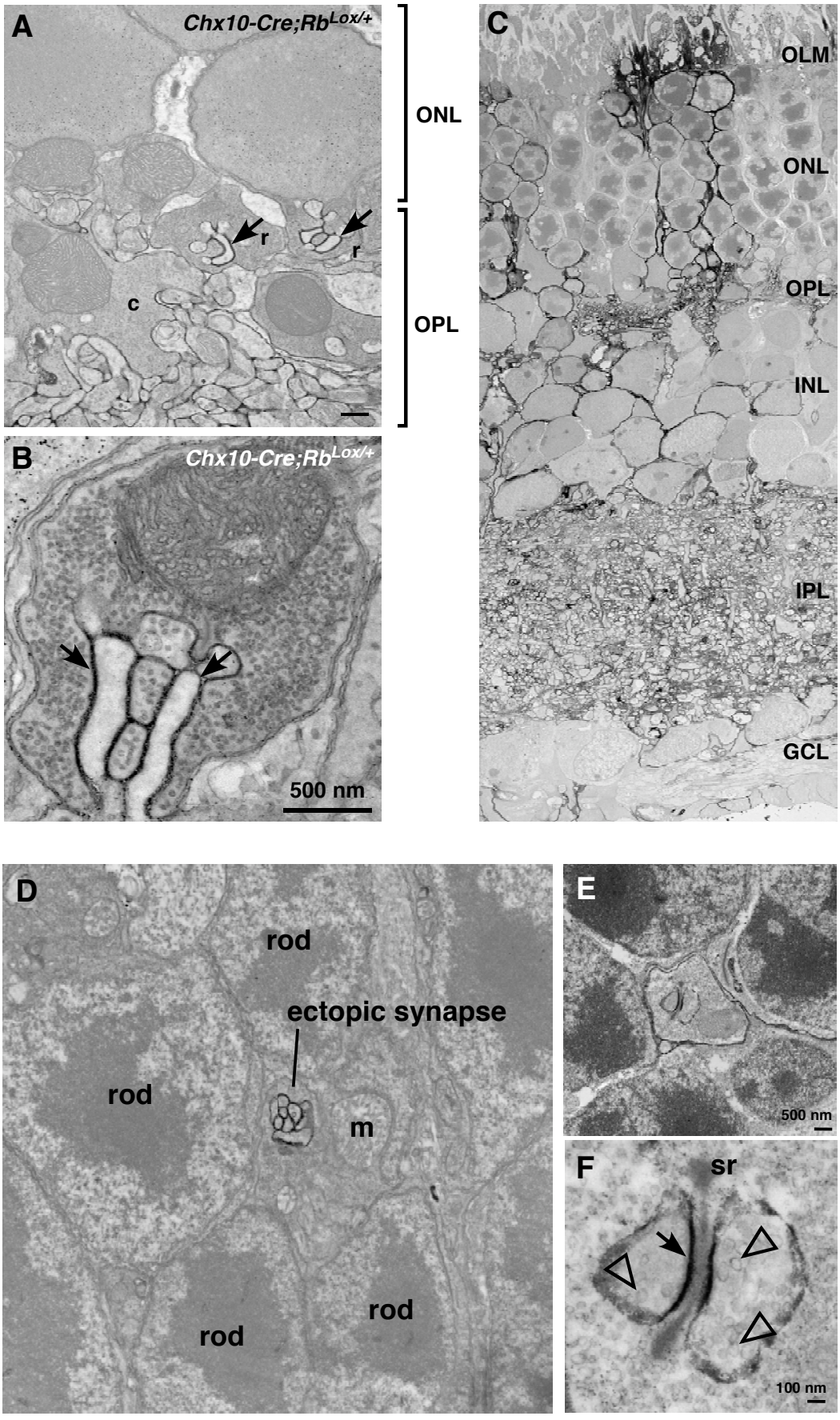

Supplemental Figure 5. Genetic mosaic analysis of synapses using AP TEM . (A) Lead citrate staining of *Chx10-Cre;Rb*$^{Lox/Lox}$*;Z/AP* retina at P21. Lead precipitate is visualized as a dark deposit at the plasma membrane on the cell bodies and neurites at the plexiform layer. Two labeled bipolar neurons (blue shading, Bip) are highlighted along with abundant labeling at the OPL apical to these cell bodies. **(B)** High magnification view of the labeled synapse in the box in (A) showing presumptive bipolar dendrites in the synaptic triad (blue shading) and horizontal processes with synaptic vesicles (green shading). **(C,D)** A lead citrate stained horizontal neuron (green shading, HC) with abundant labeling of the plexiform layer apical of this labeled cell. A high magnification view of a synaptic triad is shown in (D) highlighting the labeled horizontal cell neurites (green) containing synaptic vesicles. **(E,F)** An example of an ectopic process that is short by the criteria used in this study to define ectopic processes. This is a rare example of an ectopic process that contains labeled horizontal cell processes (arrow) and ectopic bipolar dendrites based on the absence of synaptic vesicles. Abbreviations: Bip, bipolar neuron; m, mitochondria; HC, horizontal cell; ONL, outer nuclear layer; OPL, outer plexiform layer.

Martins et al. Sup. Fig. 5

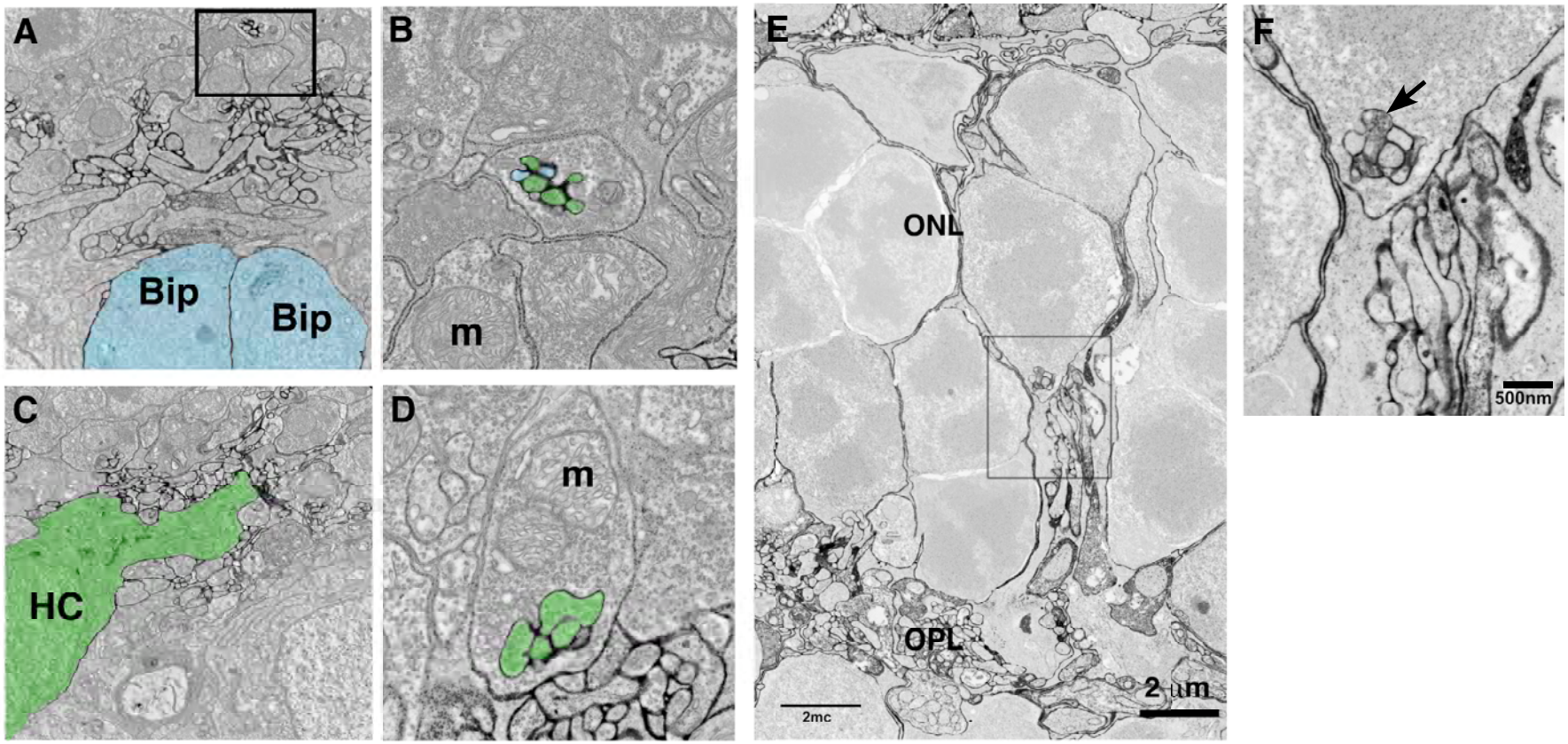

Supplemental Figure 6. Morphometric analysis of *Rb*-deficient horizontal neurons during development. (A) Scoring parameters used for this analysis. The automated algorithm allows us to extract a variety of features from the traced control and *Rb*-deficient cells including number of branch points per process, the maximum length of the process, the length of the individual elements, the average angle and the angle for each individual segment. **(B)** In an automated manner, the horizontal neurons that had apical processes were isolated and scored for branching, maximum apical process length, individual apical process length, average angle and individual angle for control and *Rb*-deficient retinae at P3 and P6. At P7 and P10-P12, we only scored the *Rb*-deficient retinae because there were no apical processes in the control retinae at these stages.

Martins et al. Sup. Fig. 6

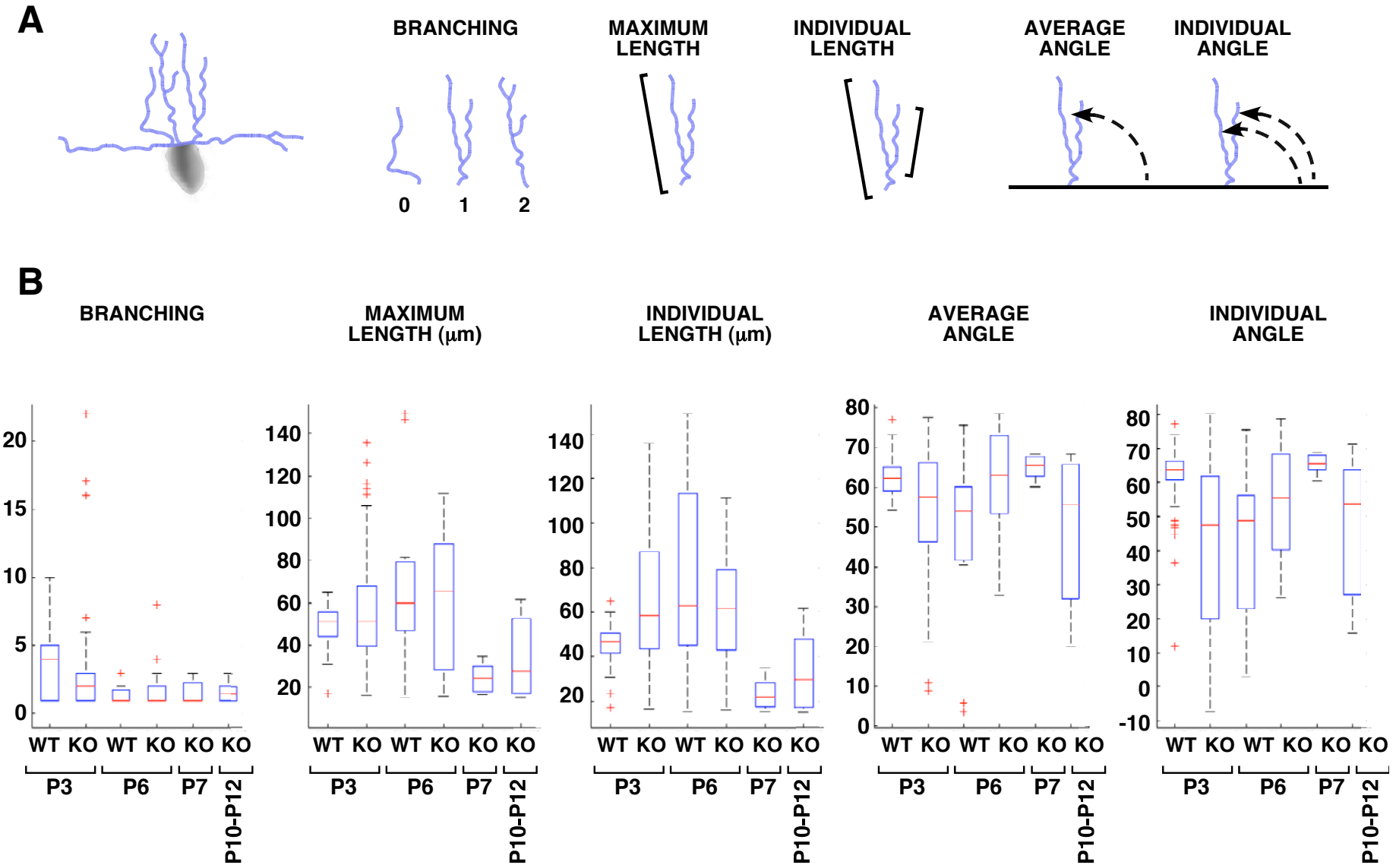

Supplemental Fig. 7. Comparison of automated and manual tracing of horizontal neurons in control and *Rb*-deficient retinae. (A-D) Using Imaris and semi-manual tracing methods, 275 cells were analyzed for each of the indicate parameters at 12 developmental stages. Mean and standard deviation is plotted for each of 3-5 individual retinae and at least 3 individual fields per retina. **(E-H)** The same datasets were analyzed using the automated algorithm. However, the greater throughput of this algorithm compared to the semi-manual method allowed us to score 906 cells in the same retinae and image sets as in (A-D).

Martins et al. Sup. Fig. 7

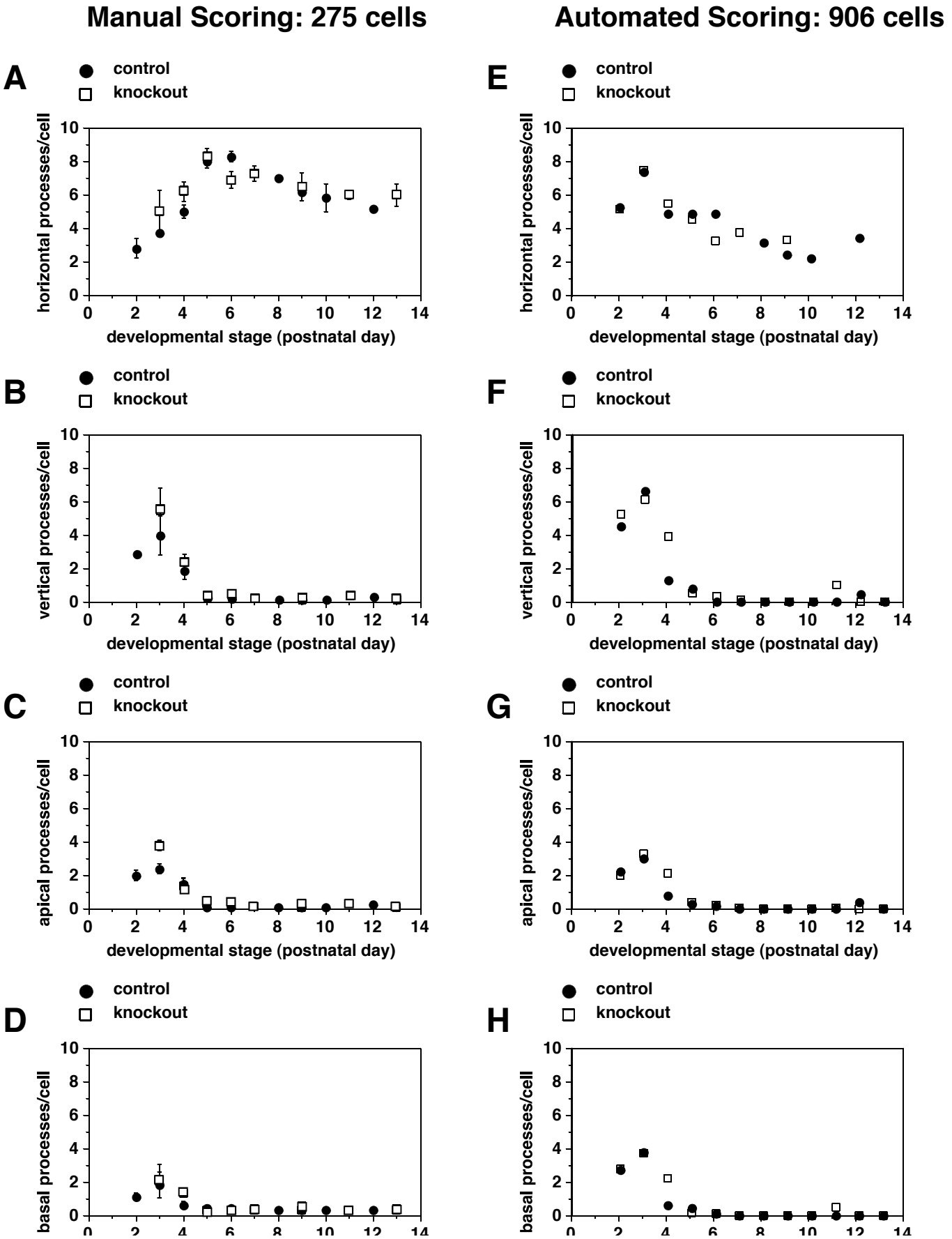

Supplemental Figure 8. Multi-photon live imaging of horizontal cells in *Chx10-Cre;Rb$^{Lox/Lox}$;Gad67-GFP* retinae. (A) Top view of one representative field with 20 horizontal cells. Arrow indicates the cells shown in **(B)**. Side view of 7 representative sequential 1 hour timepoints of a single cell with a persistent apical process (arrow) and the corresponding 3D tracing of that cell (lower panels). Apical processes are shown in red. **(A,B)** A series of images is shown for a cell with some evidence of dynamic changes in the short apical processes. None of the apical processes in this series extend 10 μm above the ONL. **(C,D)** Representative series of a horizontal neuron that matured normally and was stable over the timecourse.

Martins et al. Sup. Fig. 8

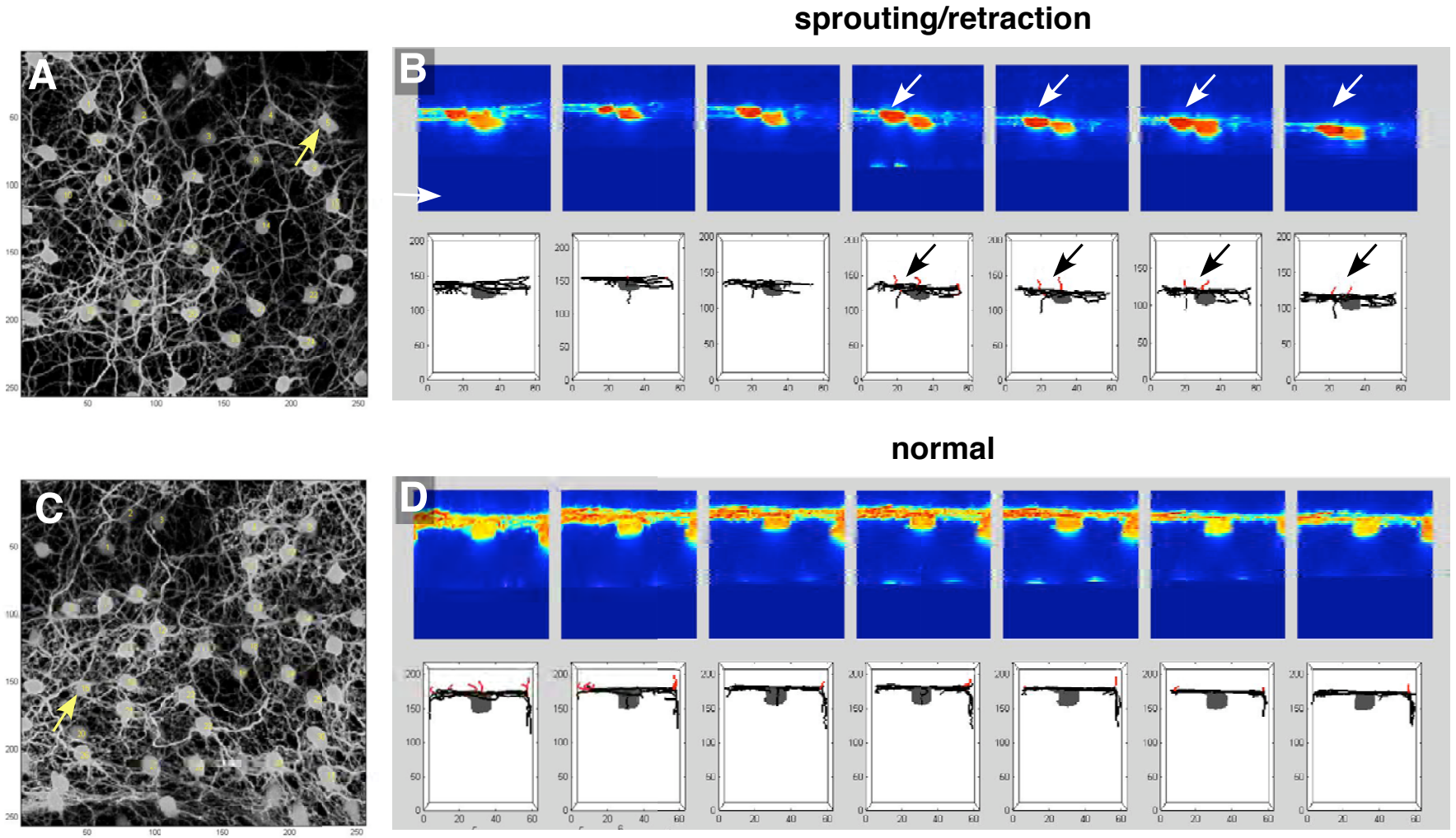

Supplemental Table 1. Contribution of Rb1-deficient horizontal processes to OPL and ectopic synapses

Location	Labeled Spherule	Labeled HC Process	Labeled Bip Dendrite	Unlabeled HC/Bip
OPL	39% (29/73)	45% (19/42)[1]	71% (30/43)[2]	32% (13/41)
ectopic	100% (28/28)	100% (28/28)	n.d.	n.d.

[1] 6 contained labeled HC process only; 13 contained both labeled HC and Bip
[2] 17 contained labeled Bip only; 13 contained both

REFERENCES

1. Johnson DA, Donovan SL, & Dyer MA (2006) Mosaic deletion of Rb arrests rod differentiation and stimulates ectopic synaptogenesis in the mouse retina. *J Comp Neurol* 498(1):112-128.
2. Contini M & Raviola E (2003) GABAergic synapses made by a retinal dopaminergic neuron. *Proc Natl Acad Sci U S A* 100(3):1358-1363.
3. Gustincich S, Feigenspan A, Wu DK, Koopman LJ, & Raviola E (1997) Control of dopamine release in the retina: a transgenic approach to neural networks. *Neuron* 18(5):723-736.